


## ORIGINAL ARTICLE

# Loss of GSTO2 contributes to cell growth and mitochondria function via the p38 signaling in lung squamous cell carcinoma

Ryusuke Sumiya<sup>1,2,3</sup>  | Masayoshi Terayama<sup>1,4</sup> | Teruki Hagiwara<sup>1</sup> | Kazuaki Nakata<sup>1</sup> | Keigo Sekihara<sup>2</sup> | Satoshi Nagasaka<sup>2</sup> | Hideki Miyazaki<sup>5</sup> | Toru Igari<sup>5</sup> | Kazuhiko Yamada<sup>3,4</sup> | Yuki I. Kawamura<sup>1</sup>

<sup>1</sup>Department of Gastroenterology, The Research Center for Hepatitis and Immunology, Research Institute, National Center for Global Health and Medicine, Chiba, Japan

<sup>2</sup>Department of Thoracic Surgery, National Center for Global Health and Medicine, Tokyo, Japan

<sup>3</sup>Course of Advanced and Specialized Medicine, Juntendo University Graduate School of Medicine, Tokyo, Japan

<sup>4</sup>Department of Surgery, National Center for Global Health and Medicine, Tokyo, Japan

<sup>5</sup>Pathology Division of Clinical Laboratory, National Center for Global Health and Medicine, Tokyo, Japan

## Correspondence

Yuki I. Kawamura, Department of Gastroenterology, The Research Center for Hepatitis and Immunology, Research Institute, National Center for Global Health and Medicine, 1-7-1 Kohnodai, 272-8516 Ichikawa, Chiba, Japan.  
Email: kawamura@hospk.ncgm.go.jp

## Present address

Masayoshi Terayama, Department of Gastroenterological Surgery, Gastroenterological Center, Cancer Institute Hospital, Japanese Foundation for Cancer Research, Tokyo, Japan

## Funding information

Japan Society for the Promotion of Science, Grant/Award Number: 19K08457 and 19K24058; National Center for Global Health and Medicine, Grant/Award Number: 19A1021, 20A1017, 20A3002 and 29-1019

## Abstract

Glutathione S-transferase omega 2 (GSTO2) lacks any appreciable GST activity, but it exhibits thioltransferase activity. The significance of GSTO2 in lung function has been reported; however, the precise expression and molecular function of GSTO2 in the lungs remain unclear. In the present study, we found that GSTO2 is expressed in airway basal cells, non-ciliated, columnar Clara cells, and type II alveolar cells, which have self-renewal capacity in the lungs. Contrastingly, no GSTO2 expression was observed in 94 lung squamous cell carcinoma (LSCC) samples. When human LSCC cell lines were treated with 5-aza-2'-deoxycytidine, a DNA-methyltransferase inhibitor, GSTO2 transcription was induced, suggesting that aberrant GSTO2 hypermethylation in LSCC is the cause of its downregulation. Forced GSTO2 expression in LSCC cell lines inhibited cell growth and colony formation *in vitro*. In a subcutaneous xenograft model, GSTO2-transfected cells formed smaller tumors in nude mice than mock-transfected cells. Upon intravenous injection into nude mice, the incidence of liver metastasis was lower in mice injected with GSTO2-transfected cells than in those injected with mock-transfected cells. In addition, GSTO2 induction suppressed the expression of  $\beta$ -catenin and the oxygen consumption rate, but it did not affect the extracellular acidification rate. Furthermore, GSTO2-transfected cells displayed lower mitochondrial membrane potential than mock-transfected cells. When GSTO2-transfected cells were treated with a p38 inhibitor,  $\beta$ -catenin expression and mitochondrial membrane potential were recovered. Our study indicated that the loss of GSTO2 via DNA hypermethylation contributes to the growth and progression of LSCC, probably by modulating cancer metabolism via the p38/ $\beta$ -catenin signaling pathway.

## KEYWORDS

cancer metabolism, GSTO2, LSCC, p38,  $\beta$ -catenin

This is an open access article under the terms of the Creative Commons Attribution-NonCommercial-NoDerivs License, which permits use and distribution in any medium, provided the original work is properly cited, the use is non-commercial and no modifications or adaptations are made.

© 2021 The Authors. *Cancer Science* published by John Wiley & Sons Australia, Ltd on behalf of Japanese Cancer Association.

## 1 | INTRODUCTION

Non-small cell lung cancer (NSCLC) is the most frequent type of lung cancer. Lung squamous cell carcinoma (LSCC) is a subtype of NSCLC, and its prognosis is poor.<sup>1</sup> The bronchi and bronchiole are covered with a variety of epithelial cell populations, such as ciliated cells, goblet cells, and Clara cells, which constitute a pseudostratified barrier that protects the lungs from infectious agents and inhaled particulates.<sup>2</sup> Airway basal cells have long-term self-renewal capacity and generate ciliated and secretory luminal cells during homeostasis and epithelial repair, and LSCC arises from airway basal cells.<sup>3</sup> Although homeostatic turnover of the bronchiolar epithelium is low compared to that in other self-renewing tissues, such as the intestine and stomach, all regions in the murine airway can be repaired after injury.<sup>4</sup> In the proximal airway, both basal and Clara cells can generate ciliated cells in the mouse bronchiole.<sup>5</sup> LSCC also arose from Clara and type II alveolar cells in a mouse model featuring genetic alterations commonly found in human LSCC, such as overexpression of *SOX2* and loss of *Cdkn2ab* and *Pten*.<sup>6</sup> Type II alveolar cells are considered the major stem cells of the distal airway and an origin of lung adenocarcinoma, another subtype of NSCLC. Molecular targeted drugs have been developed for driver mutations observed in NSCLC, such as *epidermal growth factor receptors* (*EGFR*), *anaplastic lymphoma kinase m*, and *c-ROS oncogene 1* mutations.<sup>7-9</sup> These agents are effective against lung adenocarcinoma, but they do not improve the prognosis of patients with LSCC because the aforementioned driver mutations are frequently observed in lung adenocarcinoma but not commonly present in LSCC.<sup>10</sup> For example, activating mutations of *EGFR* are present in 35% of patients with lung adenocarcinoma compared to less than 4% of patients with LSCC.<sup>11</sup> Therefore, novel anti-cancer agents based on the molecular mechanisms of LSCC carcinogenesis/progression are urgently needed.

Inhalation of toxic pollutants and microorganisms causes lung injury, which increases the risk of lung cancer. Reduced glutathione (GSH), the most abundant antioxidant expressed in the lung, plays an important role in protecting lung epithelial cells from injury and inflammation following a variety of insults.<sup>12</sup> Previous studies suggested that genetic variations of genes involved in the synthesis, modification, and activation of GSH, including *glutathione S-transferase (GST) theta 1*, *GST pi 1*, *GST mu 1*,<sup>13</sup> *GST omega 2 (GSTO2)*,<sup>14</sup> *glutamate-cysteine ligase catalytic subunit*, and *glutathione synthetase*,<sup>15</sup> contribute to the risk of chronic obstructive pulmonary disease (COPD), which is an independent risk factor for lung cancer. Among them, *GSTO2* polymorphism displayed strong associations with the primary lung function parameters forced expiratory volume in 1 second and forced vital capacity in recent genome-wide association (GWA) analyses, suggesting the significance of *GSTO2* in pulmonary function.<sup>16</sup> *GSTO2* belongs to the GST superfamily omega class, in which two *GSTO* genes have been identified in humans. In the lungs, *GSTO1* is expressed in alveolar macrophages, airway and alveolar epithelium, and extracellular fluids, including sputum supernatant.<sup>17</sup> Conversely, *GSTO2* expression in the lungs has never been elucidated under physiological or pathological conditions, such as COPD and lung cancer.

Of interest, *GSTO2* lacks any appreciable GST activity despite belonging to the GST family, which detoxifies xenobiotic substrates,

such as tobacco smoke via GSH conjugation. In contrast, *GSTO2* exhibits thioltransferase activity, which may have a potential role in regulating GSH levels.<sup>18,19</sup> In the glutathione-ascorbate cycle, redox coupling between GSH and dehydroascorbic acid influences the balance between the oxidized (NADP<sup>+</sup>) and reduced (NADPH) forms of nicotinamide adenine dinucleotide phosphate, which are converted into adenosine triphosphate (ATP) in the tricarboxylic acid (TCA) cycle to generate cellular energy. Thus, energy generation depends on oxidation and reduction reactions in mitochondria, and NADPH and GSH are indispensable for these oxidation and reduction reactions.<sup>20</sup> Therefore, *GSTO2* may have an essential role in modulating energy metabolism through the regulation of cellular redox status.

The present study aimed to clarify the significance of *GSTO2* in the lungs. In this study, we detected *GSTO2* expression in airway basal cells, Clara cells, and type II alveolar cells, which correspond to stem cells in the lungs, and loss of *GSTO2* expression was confirmed in LSCC. Upon restoring *GSTO2* expression in LSCC cells, we found that *GSTO2* suppresses cell growth both *in vitro* and *in vivo*. We also revealed that forced expression of *GSTO2* led to inhibition of mitochondrial function, suggesting that *GSTO2* plays an important role in the regulation of energy metabolism in the lungs.

## 2 | MATERIALS AND METHODS

### 2.1 | Patients

We enrolled 94 patients who received a diagnosis of LSCC and underwent lobectomy, segmentectomy, or wedge resection between January 2011 and September 2018 at the National Center for Global Health and Medicine (NCGM). This study was approved by the NCGM research ethics committee (3037), and consent was retrospectively obtained from these patients. Formalin-fixed, paraffin-embedded sections of surgical specimens were used for immunohistochemical analyses.

### 2.2 | Immunohistochemical analysis

Paraffin-embedded sections containing formalin-fixed LSCC specimens were deparaffinized and rehydrated. Target Retrieval Solution (Dako) was used to retrieve antigens. *GSTO2* immunoactivity was examined using anti-*GSTO2* antibody (HPA048141, Sigma-Aldrich), an ImmPACT DAB Peroxidase Substrate Kit (Vector Laboratories), and hematoxylin for counterstaining. Mouse anti-cytokeratin 5/6 (CK5/6) antibody (D5/16B4, Cell Marque) was used for double staining with *GSTO2*. Bound antibodies were detected using Alexa Fluor 488-conjugated goat anti-mouse IgG (for CK5/6) or TRITC-conjugated goat anti-rabbit IgG (for *GSTO2*). For the double staining with *GSTO2*, a MACH 2 Double Stain 1 Kit (Biocare Medical) and a Warp Red Chromogen Kit (Biocare Medical) were used to detect anti-CC16 (AY1E6, Hycult Biotech) and anti-surfactant protein A (SP-A; PE10, Gene Tex) signals.

### 2.3 | Cell lines and culture

LK-2 and EBC-1 human LSCC cells were obtained from the RIKEN BRC on 11 July 2018 through the National Bio-Resource Project of the MEXT. Another human LSCC cell line (H520) was purchased from American Type Culture Collection on 15 December 2020. LK-2 and H520 cells were cultured in RPMI1640 medium supplemented with 10% fetal calf serum (FCS), and EBC-1 was cultured in MEM medium supplemented with 10% FCS. In some experiments, the cells were cultured for 18 hours in a 24-well plate at a density of  $2 \times 10^4$  cells/well and then treated with 5-aza-2'-deoxycytidine (5-aza-dC, Sigma-Aldrich) for 96 hours. EBC-1 and H520 cells, which had been authenticated by the supplier using short tandem repeats (STR), were passaged in our laboratory for fewer than 6 months after resuscitation. LK-2 cells were confirmed to be the same cell line registered in the RIKEN BRC Cell Bank via comparisons with STR profiles on 19 July 2021.

### 2.4 | Bisulfite sequencing

To assess the GSTO2 methylation status, bisulfite sequencing was performed. The PCR primers used for the assay were 5'-GYGAT TTGAGATYGATTGAT-3' and 5'-CACCCRACTCCRCACCTAAA-3'. The bisulfite-PCR product was purified and cloned into a pCR4-TOPO vector (Invitrogen), and clones for subsequent sequencing were randomly selected.

### 2.5 | Ectopic expression of GSTO2

A GSTO2 expression vector was transfected into LK-2 and H520 cells using Lipofectamine LTX Reagent (Life Technologies) as previously described,<sup>21</sup> and stable transfectants were isolated using a MoFlo XDP Cell Sorter (Beckman Coulter).

### 2.6 | Quantitative RT-PCR

An RNeasy Mini Kit (QIAGEN) was used to isolate total RNA from cultured cells. A High-Capacity cDNA Reverse Transcription Kit (Applied Biosystems) was used to synthesize double-stranded cDNA. Quantitative RT-PCR was performed using ABI TaqMan probes (Applied Biosystems) as previously described. Threshold cycle numbers were determined using the Sequence Detector software and transformed with *glyceraldehyde-3-phosphate dehydrogenase* (GAPDH) as the calibrator gene according to the manufacturer's instructions. The TaqMan gene expression assay IDs for the genes used in this study were as follows: GSTO2, Hs01598184\_m1; CTNNB1, Hs00355045\_m1 and AXIN2, Hs00610344\_m1. MMP2 and VEGF $\alpha$  mRNA expression was quantified by PCR using SYBR Green PCR Master Mix (Applied Biosystems) and gene-specific primers as follows: MMP2, 5'-GAGCTCTATGGGGCTCTCC-3'

and 5'-CGTCACAGTCCGCCAAATGA-3'; and VEGF $\alpha$ , 5'-TTTCT GCTGTCTTGGGTGCATTGG-3', and 5'-ACCACTTCGTGATGA TTCTGCCCT-3'.

### 2.7 | Cell proliferation assays and colony formation assays

Viable LK-2 and H520 transfectants ( $2 \times 10^3$  cells/well) were seeded into 96-well plates, and cell proliferation was measured using an MTT assay kit (Nacalai Tesque). For the colony formation assays, LK-2 and H520 (200 cells/well) transfectants were seeded into 24-well plates. After incubation for 2 weeks, colonies were stained with crystal violet.

### 2.8 | Xenograft model in athymic mice

Male BALB/c nude (nu/nu) mice were purchased from CLEA Japan and maintained under pathogen-free conditions in the animal facility of the NCGM. Vector-transfected and GSTO2-transfected cells ( $5.0 \times 10^6$ ) were injected subcutaneously into the right and left flanks of 6-week-old BALB/c nude mice, respectively (N = 8/group). After 14 days, tumor size was measured using calipers. Tumor volume was determined using the long (a) and short (b) diameters and height (c) as follows: volume =  $a \times b \times c \times 3.14/6$ . In the liver metastasis model, vector-transfected and GSTO2-transfected cells ( $5.0 \times 10^6$ ) were injected intravenously into the tail vein of 6-week-old BALB/c nude mice (N = 8/group). After 8 weeks, the number of hepatic tumors was measured. All experiments were performed with prior approval from the Animal Experimentation Committee of NCGM.

### 2.9 | Quantification of p38 phosphorylation and $\beta$ -catenin

Cultured LK-2 and H520 transfectants ( $5 \times 10^4$  cells/well) in a poly-L-lysine-coated slide chamber (Iwaki) were stained with anti-phospho-p38 mitogen-activated protein kinase (MAPK) antibody (Cell Signaling Technology) or anti-human  $\beta$ -catenin antibody (Santa Cruz Biotechnology) as previously described.<sup>21</sup> Images were captured using a confocal microscopy system (FV-1000, Olympus). In some experiments, the cells were treated with SB203580 (p38 inhibitor; Calbiochem) for 24 hours.

### 2.10 | Oxidative phosphorylation and glycolysis analysis

The real-time extracellular acidification rate (ECAR) and oxygen consumption rate (OCR) were analyzed using an XF96 metabolic flux analyzer (Seahorse Biosciences), and the obtained data were assessed using Seahorse XF96 Wave software (Seahorse Biosciences) according

to the manufacturer's instructions. Briefly, LK-2 ( $6 \times 10^4$ ) and H520 transfectants ( $4 \times 10^4$ ) were seeded into each well of a Seahorse XF96 cell culture microplate. For OCR, 1 mmol/L oligomycin, 1 mmol/L carbonyl cyanide p-(trifluoromethoxy) phenylhydrazone (FCCP), and 2 mmol/L antimycin A plus 2 mmol/L rotenone were sequentially injected, and for ECAR, 10 mmol/L glucose, 1 mmol/L oligomycin, and 80 mmol/L 2-deoxyglucose (2-DG) were sequentially injected.

### 2.11 | Mitochondrial membrane potential assay

Live cell imaging was performed using JC-1 (5, 5', 6, 6'-tetrachloro-1, 1', 3, 3'-tetraethylbenzimidazolylcarbocyanine iodide, Thermo Fisher Scientific) to assess the mitochondrial membrane potential. Briefly, LK-2 and H520 transfectants were incubated with JC-1 dye at a concentration of 5  $\mu\text{g/mL}$  for 30 minutes at 37°C. Images of dye-loaded cells were captured using an In Cell Analyzer (Carl Zeiss).

### 2.12 | Statistical analysis

The data were expressed as the mean  $\pm$  SD, and the results were compared using paired or unpaired Student's *t* tests. Statistical analyses were performed using the Prism 8 statistical program (GraphPad Software). All tests were two-tailed, and *P* < .05 denoted statistical significance.

## 3 | RESULTS

### 3.1 | GSTO2 expression was suppressed by aberrant DNA hypermethylation in lung squamous cell carcinoma

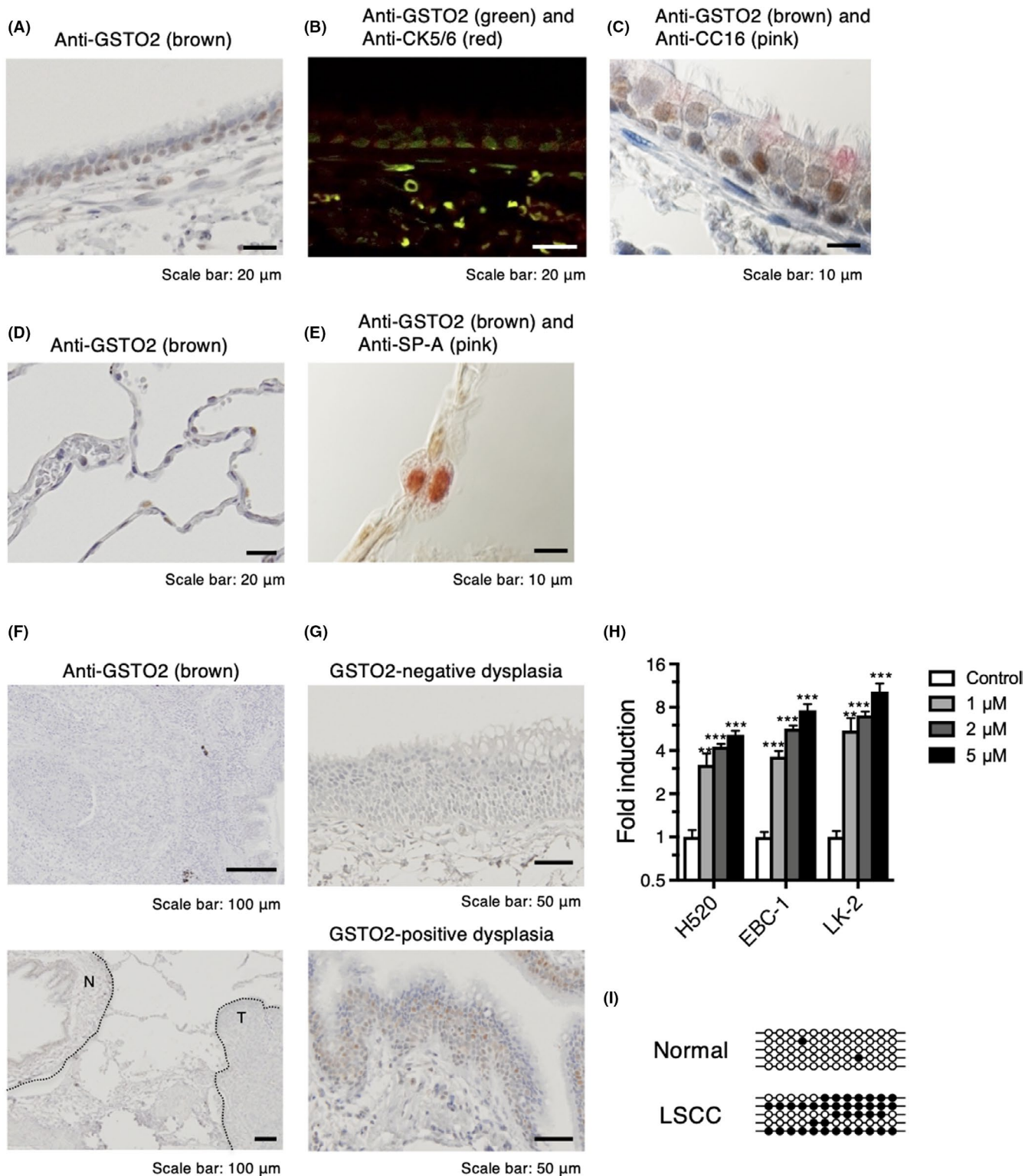
To investigate the protein expression and localization of GSTO2 in normal lung and LSCC specimens, immunohistochemical analyses were performed. In the normal bronchial epithelium, GSTO2 protein was detected in the nuclei of most basal cells (Figure 1A). Specific GSTO2 expression in airway basal cells was confirmed by double staining for GSTO2 and CK5/6, which is a marker of airway basal cells<sup>22</sup> (Figure 1B). In addition, we detected GSTO2 expression in a minor population of non-basal epithelial cells in the bronchi and bronchiole. This was clearly

visualized by double staining for GSTO2 and CC16, which is secreted by the non-ciliated Clara cells in the bronchi and bronchiole,<sup>23</sup> illustrating that GSTO2 protein was also expressed in Clara cells (Figure 1C). In the normal alveoli, GSTO2 protein was detected in alveolar type II cells (Figure 1D), which was confirmed by double staining for GSTO2 and SP-A, a lung-specific glycoprotein in pulmonary surfactant that is secreted by alveolar type II cells<sup>24</sup> (Figure 1E). GSTO2 expression was detected in 80% of normal tissues surrounding the LSCC (Table 1). In contrast, all 94 LSCC specimens examined in this study displayed no GSTO2 expression in an immunohistochemical analysis (Figure 1F). LSCC is classified according to the location of the tumor into either a central or a peripheral type, and the clinicopathologic features of LSCC are significantly different between the two types.<sup>25</sup> Our present study enrolled both LSCC types; therefore, loss of GSTO2 occurred in central LSCC and peripheral LSCC. Loss of GSTO2 was also observed in 60% of dysplasia, which is the precancerous lesion of LSCC (Figure 1G and Table 1). To examine whether DNA methylation of the GSTO2 could explain the loss of GSTO2 expression in LSCC, we measured endogenous GSTO2 mRNA expression in three LSCC cell lines and compared them with the expression in cells treated with 5-aza-dC, a DNA methyltransferase inhibitor. In all cell lines, treatment with 5-aza-dC resulted in increased GSTO2 mRNA expression (Figure 1H). The methylation status of GSTO2 was assessed using bisulfite sequencing. As expected, methylated CpGs were hardly detected in normal tissues, whereas it was evident that the promoter region of the GSTO2 was frequently hypermethylated in LSCC tissues (Figure 1I). These results indicate that GSTO2 expression was silenced by DNA hypermethylation in LSCC.

### 3.2 | Forced GSTO2 expression inhibited cell growth *in vitro* and *in vivo*

To clarify the function of GSTO2, we prepared GSTO2-transfected and mock-transfected LK-2 and H520 cells and examined the effect of GSTO2 expression on their growth. Stably GSTO2-transfected LK-2 and H520 cells displayed >1500- and 25-fold higher GSTO2 expression than their mock-transfected counterparts, respectively (Figure 2A). In both cell lines, GSTO2 overexpression significantly inhibited cell growth compared to the findings in the mock transfectants (Figure 2B). In the colony formation assay, GSTO2 transfectants of both LSCC cell lines failed to form colonies, whereas mock transfectants formed colonies efficiently (Figure 2C). Finally, GSTO2- and

**FIGURE 1** Glutathione S-transferase omega 2 (GSTO2) expression was restricted to basal cells, Clara cells, and type II alveolar cells in normal lung tissues but was lost in lung squamous cell carcinoma (LSCC). (A) A representative image of normal bronchial samples stained with anti-GSTO2. (B) A representative image of normal bronchial samples double-stained with anti-GSTO2 (green) and anti-CK5/6 (red). (C) A representative image of normal bronchial samples double-stained with anti-GSTO2 (brown) and anti-CC16 (pink). (D) A representative image of normal alveolar samples stained with anti-GSTO2. (E) A representative image of normal alveolar samples double-stained with anti-GSTO2 (brown) and anti-SP-A (pink). (F) Representative images of LSCC alone (upper) and LSCC surrounded by normal tissues (lower) stained with anti-GSTO2 antibody. N, normal; T, tumor. (G) Immunohistochemical analysis of GSTO2 expression in dysplasia. Representative staining of GSTO2-negative (upper) and GSTO2-positive (lower) samples. (H) The mRNA induction of GSTO2 in LSCC cell lines after treatment with 1, 2, or 5  $\mu\text{mol/L}$  5-aza-dC. Data are reported as the fold increases in induction relative to that in untreated cells and presented as the mean  $\pm$ SD of assays performed in triplicate. \*\**P* < .01, \*\*\**P* < .001. (I) Methylation status of individual CpG residues in the GSTO2 gene in normal and LSCC samples as determined by bisulfite sequencing. Bisulfite PCR products cloned into the pCR4-TOPO vector were randomly selected for sequencing. Each line indicates an independent clone from bisulfite-PCR products containing 12 consecutive CpGs. The filled circles on the lines for each clone represent methylated CpGs, whereas open circles represent unmethylated CpGs



mock-transfected LK-2 cells were used in a subcutaneous xenograft model of tumor formation in BALB/c nude mice. GSTO2 transfectants formed smaller tumors than mock transfectants (Figure 2D). Cell growth *in vivo* was further assessed in an intravenous injection model. When GSTO2 transfectants were injected intravenously into nude mice, the number of hepatic tumors was lower than that in mock-transfected cells (Figure 2E). Collectively, these results demonstrate that GSTO2 expression inhibits LSCC growth *in vitro* and *in vivo*.

### 3.3 | Forced GSTO2 expression inhibited the expression of $\beta$ -catenin via p38 phosphorylation

Our previous study demonstrated that GSTO2 regulates  $\beta$ -catenin expression via p38 phosphorylation in esophageal squamous cell carcinoma (ESCC).<sup>21</sup> Because  $\beta$ -catenin has diverse physiological functions, including involvement in many cancer-related processes,<sup>26</sup> we next examined whether GSTO2 expression affects p38 phosphorylation

TABLE 1 The GSTO2 expression in normal, dysplasia, and LSCC

|           | Total | GSTO2 expression |           | P-value  |
|-----------|-------|------------------|-----------|----------|
|           |       | Disappeared      | Expressed |          |
| Normal    | 81    | 16 (20%)         | 65 (80%)  |          |
| Dysplasia | 70    | 42 (60%)         | 28 (40%)  | <0.0001* |
| LSCC      | 94    | 94 (100%)        | 0 (0%)    | <0.0001* |

Note: The ratio of GSTO2 loss in dysplasia and LSCC was compared with that in normal tissues using the  $\chi^2$  test. \*shows statistical significance. LSCC, lung squamous cell carcinoma.

and  $\beta$ -catenin expression in LSCC. In both cell lines used, p38 phosphorylation was accelerated in GSTO2-transfected cells compared to that in mock-transfected cells (Figure 3A). Furthermore, we examined the association between GSTO2 expression and p38 phosphorylation in normal bronchial epithelium and detected phosphorylated p38 in airway basal cells (Figure 3B) and Clara cells (Figure 3C), which specifically expressed GSTO2 in normal tissues (Figure 1A-C). Moreover, overexpression of GSTO2 suppressed the protein expression of  $\beta$ -catenin (Figure 3D). As expected, no changes in  $\beta$ -catenin mRNA expression were induced by GSTO2 overexpression (Figure 3E), which

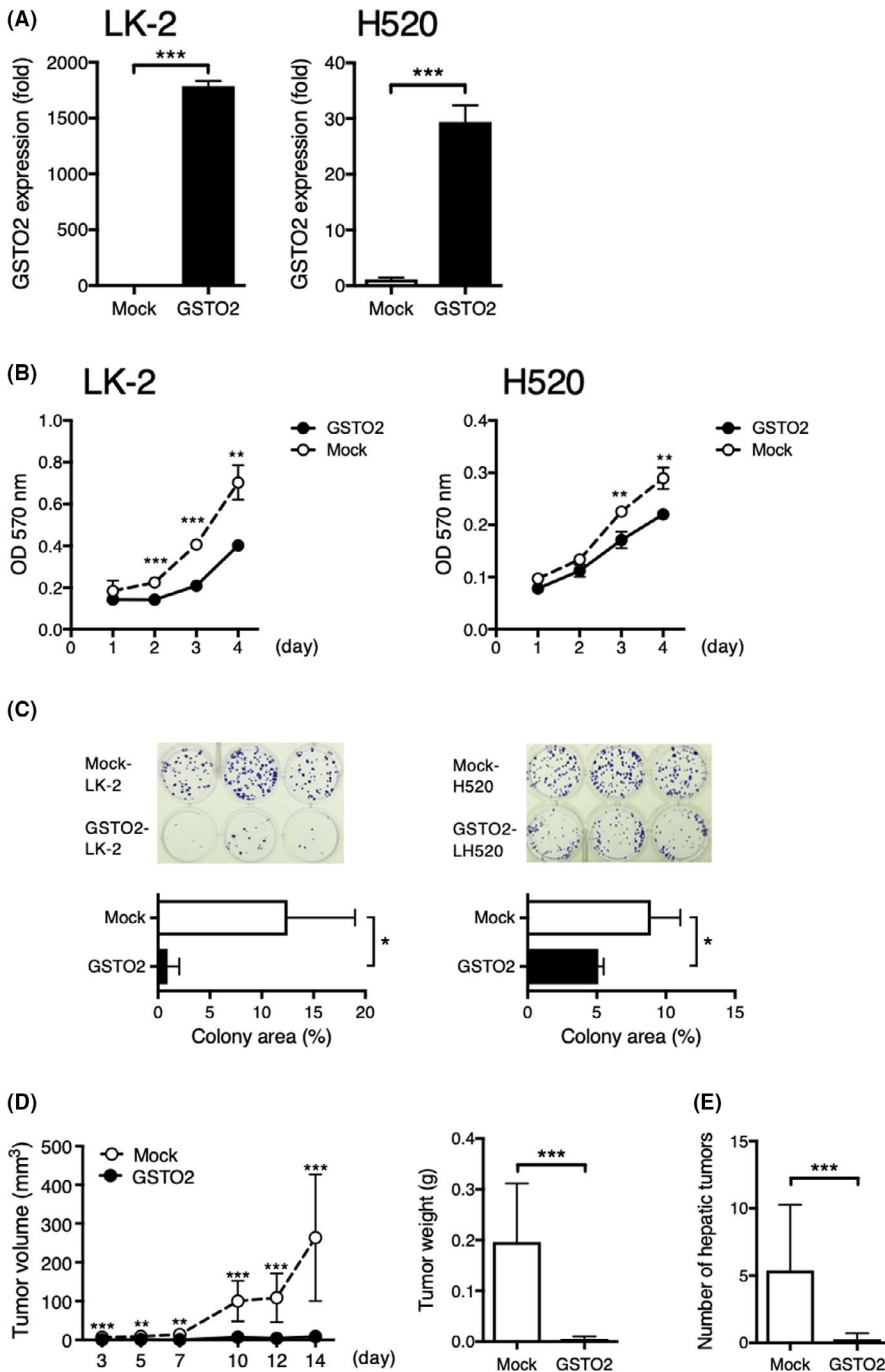


FIGURE 2 Ectopic expression of GSTO2 suppressed cell growth *in vitro* and *in vivo*. (A) GSTO2 mRNA levels in mock-transfected and GSTO2-transfected cells. (B) Growth curves of GSTO2-transfected and mock-transfected cells as determined using the MTT assay. Data are presented as the mean  $\pm$ SD of assays performed in triplicate. \*\* $P < .01$ , \*\*\* $P < .0001$ . (C) GSTO2-transfected and mock-transfected cells were cultured for 2 wk. Representative images of colonies visualized with crystal violet staining (upper panels). The area of colonies was measured in three separate wells, and the results are presented as the mean  $\pm$ SD (lower panels). \* $P < .05$ . (D) Nude mice were subcutaneously inoculated with GSTO2-transfected LK-2 cells in the left flank and mock-transfected LK-2 cells in the right flank, and tumor volumes were quantified (left). Fourteen days after inoculation, tumor weights were measured (right). \*\* $P < .01$ , \*\*\* $P < .0001$ . (E) Nude mice were intravenously inoculated with GSTO2-transfected LK-2 cells or mock-transfected LK-2 cells. Eight weeks after inoculation, the number of hepatic tumors was counted. \*\*\* $P < .0001$

is concordant with our previous report that *GSTO2* overexpression caused post-transcriptional downregulation of  $\beta$ -catenin in ESCC, probably via enhanced p38 phosphorylation.<sup>21</sup> Therefore, we further examined the involvement of the p38 signaling pathway in the *GSTO2*-mediated downregulation of  $\beta$ -catenin in LSCC using a p38 inhibitor. When *GSTO2*-transfected cells were treated for 24 hours with SB203580, a specific inhibitor of the p38 MAPK pathway,  $\beta$ -catenin expression was restored (Figure 3A), suggesting that the downregulation of  $\beta$ -catenin caused by *GSTO2* overexpression is mediated by the enhancement of p38 phosphorylation. In addition, we observed a significant reduction in the nuclear expression of  $\beta$ -catenin upon *GSTO2* overexpression in LSCC (Figure 3D). Because nuclear  $\beta$ -catenin is known to act as a transcriptional factor that modulates gene expression in carcinogenesis through the induction of cancer stem cell features, bulk tumor proliferation, and EMT,<sup>26</sup> we speculated that *GSTO2* expression inhibits LSCC growth by modulating  $\beta$ -catenin-dependent gene transcription. We examined whether *GSTO2* expression in LSCC affects the transcription of *AXIN2*, *VEGF $\alpha$* , and *MMP2*, the expression of which is known to be regulated by  $\beta$ -catenin<sup>27</sup>; however, changes in the mRNA levels of these  $\beta$ -catenin-targeted genes in these cell lines were inconsistent. For example, in *GSTO2*-transfected H520 cells, *AXIN2* and *VEGF $\alpha$*  mRNA expression was significantly lower than that in mock-transfected H520 cells, whereas the transcription of *AXIN2* in *GSTO2*-transfected LK-2 was rather accelerated compared to that in mock-transfected LK-2 cells (Figure 3F). These results collectively suggest that growth suppression caused *GSTO2* expression might not result from the modulation of  $\beta$ -catenin-dependent gene transcription.

### 3.4 | Forced *GSTO2* expression inhibited the mitochondrial function via p38 phosphorylation

Recently, a novel function of  $\beta$ -catenin in mitochondrial metabolism as a regulator of the TCA cycle and oxidative phosphorylation (OXPHOS) was reported in hepatocytes.<sup>28</sup> Therefore, we examined the effect of *GSTO2* expression on mitochondrial metabolism in LSCC. Metabolomic analyses using the XF96 extracellular flux analyzer revealed that *GSTO2* did not affect aerobic glycolysis, as assessed by ECAR in LK-2 and H520 cells. In contrast, *GSTO2* overexpression in both cell lines used suppressed mitochondrial respiration (OCR; Figure 4A). Mitochondrial function was further assessed using mitochondrial membrane potential via JC-1 dye staining. In both cell lines used, *GSTO2* overexpression facilitated depolarization of the mitochondria membrane (Figure 4B). Finally, we examined the involvement of the p38 signaling pathway in the *GSTO2*-mediated modulation of mitochondrial function in LSCC and confirmed that SB203580 treatment of *GSTO2*-transfected cells restored mitochondria membrane potential; conversely, SB203580 did not affect mitochondria membrane potential in mock-transfected cells (Figure 4B). These results collectively suggest that *GSTO2* overexpression attenuates mitochondrial membrane potential, probably via the p38/ $\beta$ -catenin axis.

## 4 | DISCUSSION

In this study, we demonstrated for the first time that *GSTO2* is expressed in the bronchial basal cells, Clara cells, and type II alveolar cells, which correspond to stem cells in the lungs, and the loss of *GSTO2* in LSCC was confirmed. We also illustrated the function of *GSTO2* in regulating cell growth,  $\beta$ -catenin expression, and mitochondrial respiration through p38 phosphorylation.

The lungs comprise a complex organ consisting of anatomically distinct regions, such as the trachea, bronchioles, and alveoli, and they contain numerous putative stem cell populations that contribute to region-specific tissue homeostasis and repair.<sup>7-10</sup> The results of this study demonstrated that *GSTO2* is expressed in all types of pulmonary stem cells, such as airway basal cells, Clara cells, and type II alveolar cells. Together with the previous report of GWA analyses revealing a strong association between a non-synonymous coding SNP in *GSTO2* and lung function,<sup>18</sup> *GSTO2* may have indispensable roles in the maintenance of stemness and pulmonary function in each region of the lungs. Furthermore, loss of *GSTO2* via DNA hypermethylation may disrupt tissue homeostasis and eventually cause malignant transformation because lung cancers, similarly to other types of cancers, are believed to arise from stem cells.<sup>7,10,21</sup> Epigenetic silencing of *GSTO2* by DNA hypermethylation has never been reported, excluding our recent study in ESCC.<sup>29</sup> Smoking, one of the major risk factors for LSCC and ESCC, causes aberrant DNA methylation and eventually abnormal gene expression.<sup>30</sup> In addition, *GSTO2* variation may also affect its expression level because *GSTO2* variants carrying SNP associated with COPD risk and lung function displayed decreased protein expression in COS-1 cells compared to the wild-type level.<sup>31</sup>

Another important finding of this study was that *GSTO2* regulates cell growth and  $\beta$ -catenin expression. Furthermore, we suggest that p38 activation is required for *GSTO2*-induced  $\beta$ -catenin downregulation. To the best of our knowledge, there are no reports demonstrating that *GSTO2* serves as the kinase of p38 MAPK. A previous study revealed that treatment of fetal alveolar type II cells with N-acetyl-L-cysteine, a GSH precursor, reduced p38 phosphorylation levels concomitantly with the induction of intracellular GSH.<sup>32</sup> This indicates that *GSTO2* activated p38 MAPK, not via direct phosphorylation rather probably due to the modulation reduced GSH/oxidized GSH balance. Jie et al reported the role of p38 signaling in regulating  $\beta$ -catenin during osteoclastogenesis. In this report, p38 phosphorylation promoted phosphorylation of  $\beta$ -catenin at S33, which marks  $\beta$ -catenin for degradation through ubiquitin-mediated mechanisms.<sup>33</sup> Whether the phosphorylation of  $\beta$ -catenin at this site and the ubiquitination of  $\beta$ -catenin were induced by *GSTO2* overexpression should be elucidated, but our data may suggest that *GSTO2* is one of the regulators of  $\beta$ -catenin-mediated signaling. Once  $\beta$ -catenin escapes from degradation, it accumulates in the cytoplasm and then shuttles to the nucleus.<sup>27,28,34</sup> Indeed, cytoplasmic and nuclear localization of  $\beta$ -catenin has been observed in LSCC.<sup>35</sup> In

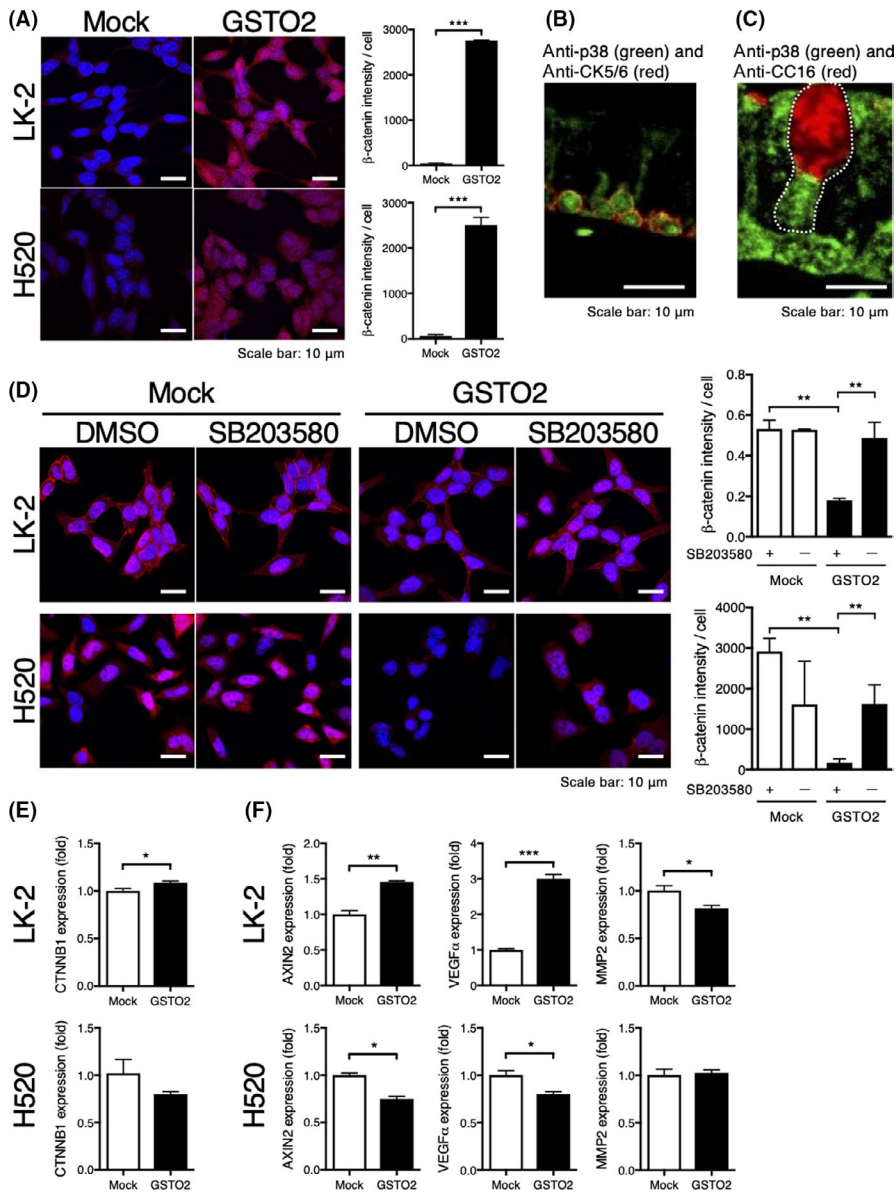


**FIGURE 3** Ectopic expression of GSTO2 downregulated  $\beta$ -catenin through p38 phosphorylation. (A) Left: Typical images of mock-transfected and GSTO2-transfected cells. Phosphorylated p38 (red) was visualized by nuclear staining (blue). p38 phosphorylation per nucleus was quantified and presented as the mean  $\pm$ SD of assays performed in triplicate. \*\*\* $P < .001$ . (B) A representative image of normal bronchial samples double-stained with anti-p38 (green) and anti-CK5/6 (red). (C) A representative image of normal bronchial samples double-stained with anti-p38 (green) and anti-CC16 (red). The Clara cell is surrounded by a dotted line. (D) Left: Typical images of mock-transfected and GSTO2-transfected cells after treatment with 50  $\mu$ mol/L SB203580 or DMSO for 24 h.  $\beta$ -catenin (red) was visualized by nuclear staining (blue).  $\beta$ -catenin expression per nucleus was quantified and presented as the mean  $\pm$ SD of assays performed in triplicate. \*\* $P < .01$ . (E) CTNNB1 mRNA levels in mock-transfected and GSTO2-transfected cells. Data are presented as the mean  $\pm$ SD of assays performed in triplicate. \* $P < .05$ . (F) Transcript levels of AXIN2, VEGF, and MMP2 were determined by quantitative RT-PCR in mock-transfected and GSTO2-transfected cells. Data are presented as the mean  $\pm$ SD of assays performed in triplicate. \* $P < .05$ , \*\* $P < .01$ , \*\*\* $P < .001$

nuclei,  $\beta$ -catenin acts as a key nuclear effector of the major (canonical) Wingless-type protein pathway and modulates the expression of genes involved in lung carcinogenesis/progression.<sup>36</sup> However, its biological rule in LSCC did not coincide with previous reports because our data suggest that GSTO2-induced  $\beta$ -catenin downregulation in nuclei did not suppress the transcription of  $\beta$ -catenin-targeted genes. Previous research demonstrated that  $\beta$ -catenin-deficient hepatocytes exhibited mitochondrial dysfunction and decreased ATP production, suggesting a pivotal role of  $\beta$ -catenin in mitochondrial metabolism as a regulator of the TCA cycle and OXPHOS. In  $\beta$ -catenin-deficient hepatocytes, induction of redox imbalance accelerated the deterioration of mitochondrial function, including reduced OXPHOS and ATP production.<sup>28</sup> To clarify whether GSTO2 expression induced redox imbalance, we measured GSH oxidation, NAD<sup>+</sup>/NADH, and NADP<sup>+</sup>/NADPH in mock-transfected and GSTO2-transfected cells. We found no evidence that GSTO2 influences the balance of redox coupling in

the glutathione-ascorbate cycle and TCA cycle (data not shown). Although technically difficult, the roles of these substrates of oxidation and reduction reactions must be assessed separately between cytosolic and mitochondrial pools because their cellular pools are compartmentalized<sup>34</sup> and GSTO2 may affect either one. Meanwhile, GSTO2 overexpression did not affect aerobic glycolysis. It has been reported that cancer cells depend on aerobic glycolysis rather than on mitochondrial OXPHOS, also known as the "Warburg effect".<sup>37</sup> However, recent reports indicated that mitochondrial OXPHOS is not always suppressed in cancer cells, even in the presence of oxygen, and it is also utilized as fuel for tumorigenesis.<sup>37</sup> Our results indicated that LSCC can utilize mitochondrial OXPHOS to produce ATP, and the loss of GSTO2 may contribute to the growth of LSCC by modulating mitochondrial metabolism.

To our knowledge, this study presents the first evidence that GSTO2 is exclusively expressed in a variety of stem cells in the lungs



**FIGURE 4** Ectopic expression of *GSTO2* inhibited mitochondrial function through p38 phosphorylation. (A) ECAR (left) and OCR (middle) were measured using an Extracellular Flux Analyzer in four or five separate wells, and the results are presented as the mean  $\pm$ SD. Injection A = glucose; B = oligomycin; C = 2-DG; D = FCCP; E = antimycin A + rotenone. The red line denotes mock-transfected cells, and the blue line denotes *GSTO2*-transfected cells. The maximum OCRs are presented as the mean  $\pm$ SD (right). \* $P < .05$ , \*\* $P < .01$ . (B) Mitochondrial membrane potential of mock-transfected and *GSTO2*-transfected cells after treatment with 50  $\mu$ mol/L SB203580 or DMSO for 24 h was assessed using JC-1 assay. JC-1 signals per nucleus were quantified and presented as the mean  $\pm$ SD of assays performed in triplicate. \* $P < .05$ , \*\* $P < .01$ , \*\*\* $P < .001$

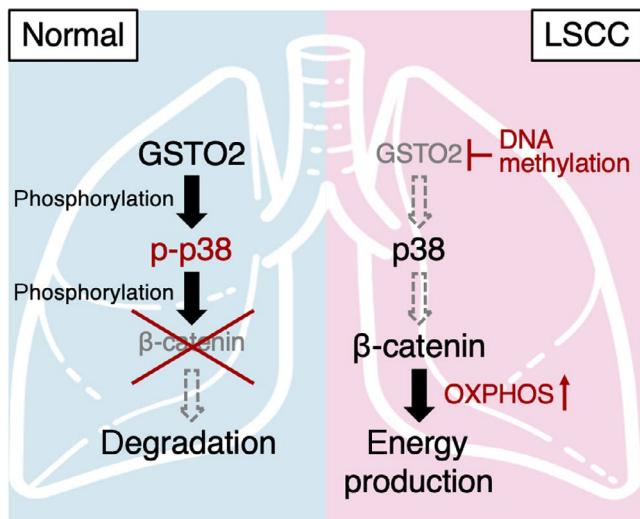
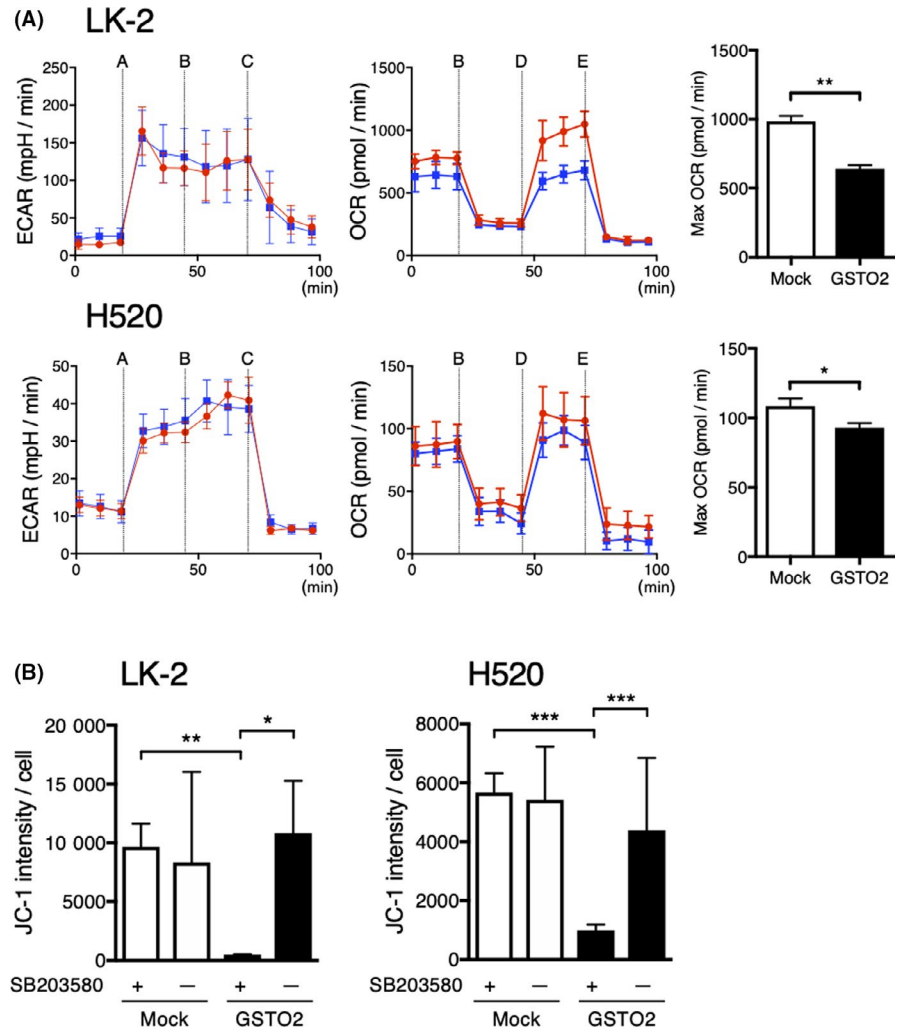


**FIGURE 5** Role of *GSTO2* in normal lung and LSCC cells. In normal lung cells, *GSTO2* activates the p38 mitogen-activated protein kinase (MAPK), which results in decrease  $\beta$ -catenin expression probably via ubiquitination. By contrast, silencing of *GSTO2* is caused by DNA hypermethylation in LSCC, which allows  $\beta$ -catenin to escape from degradation, activate mitochondrial OXPHOS, and promote energy production

but that its expression is silenced by DNA hypermethylation in LSCC. In addition, these findings shed light on the pivotal role of *GSTO2* as a regulator for  $\beta$ -catenin via the p38 signaling pathway. In normal lungs, *GSTO2* activates p38 MAPK, resulting in  $\beta$ -catenin downregulation, probably via ubiquitination. By contrast, silencing of *GSTO2* is caused by DNA hypermethylation in LSCC, which allows  $\beta$ -catenin to escape from degradation, activate mitochondrial OXPHOS, and promote energy production (Figure 5). Our findings may have important implications for the prevention of LSCC.

#### ACKNOWLEDGMENTS

We thank Drs Miwa Tamura-Nakano and Chinatsu Oyama at the NCGM EM Support Unit for their technical support in histological analysis, Mr Naoki Kashiwagi (Olympus) for technical assistance with cell imaging, and Mr Yasuhiko Nagasaka (Beckman Coulter) for technical assistance with cell sorting. We also thank Ms Yasuko Nozaki for her technical assistance. The authors would like to thank Enago for the English language review. This study was supported by grants-in-aid for research from the National Center for Global Health and Medicine (29-1019 to KY and YIK, 19A1021 to KS, SN and YIK, 20A1017 to KY and YIK, 20A3002 to RS); JSPS KAKENHI Grants (19K08457 to YIK, 19K24058 to MT).

## CONFLICT OF INTEREST

The authors have no conflicts of interest to declare.

## ORCID

Ryusuke Sumiya  <https://orcid.org/0000-0002-2464-6717>

## REFERENCES

- Wang BY, Huang JY, Chen HC, et al. The comparison between adenocarcinoma and squamous cell carcinoma in lung cancer patients. *J Cancer Res Clin Oncol*. 2020;146:43-52.
- Cole BB, Smith RW, Jenkins KM, Graham BB, Reynolds PR, Reynolds SD. Tracheal basal cells: a facultative progenitor cell pool. *Am J Pathol*. 2010;177:362-376.
- Hynds RE, Janes SM. Airway basal cell heterogeneity and lung squamous cell carcinoma. *Cancer Prev Res (Phila)*. 2017;10:491-493.
- Hogan BLM, Barkauskas CE, Chapman HA, et al. Repair and regeneration of the respiratory system: complexity, plasticity, and mechanisms of lung stem cell function. *Cell Stem Cell*. 2014;15:123-138.
- Rawlins EL, Okubo T, Xue Y, et al. The role of Scgb1a1+ Clara cells in the long-term maintenance and repair of lung airway, but not alveolar, epithelium. *Cell Stem Cell*. 2009;4:525-534.
- Ferone G, Song JY, Sutherland KD, et al. SOX2 is the determining oncogenic switch in promoting lung squamous cell carcinoma from different cells of origin. *Cancer Cell*. 2016;30:519-532.
- Rafei H, El-Bahesh E, Finianos A, Nassereddine S, Tabbara I. Immune-based therapies for non-small cell lung cancer. *Anticancer Res*. 2017;37:377-387.
- Goldstraw P, Ball D, Jett JR, et al. Non-small-cell lung cancer. *Lancet*. 2011;378:1727-1740.
- Sholl LM. Biomarkers in lung adenocarcinoma: a decade of progress. *Arch Pathol Lab Med*. 2015;139:469-480.
- Li Y, Xu F, Zhu Q, Ge D, Lu C. Transcriptomic and functional network features of lung squamous cell carcinoma through integrative analysis of GEO and TCGA data. *Sci Rep*. 2018;8:15834.
- Wang R, Zhang Y, Pan Y, et al. Comprehensive investigation of oncogenic driver mutations in Chinese non-small cell lung cancer patients. *Oncotarget*. 2015;6:34300-34308.
- Rooney C, Sethi T. The epithelial cell and lung cancer: the link between chronic obstructive pulmonary disease and lung cancer. *Respiration*. 2011;81:89-104.
- Cheng SL, Yu CJ, Yang PC. Genetic polymorphism of epoxide hydrolase and glutathione S-transferase in COPD. *Eur Respir J*. 2004;23:818-824.
- Yanbaeva DG, Wouters EFM, Dentener MA, Spruit MA, Raynaert NL. Association of glutathione-S-transferase omega haplotypes with susceptibility to chronic obstructive pulmonary disease. *Free Radic Res*. 2009;43:738-743.
- Andrade M, Li Y, Marks RS, et al. Genetic variants associated with the risk of chronic obstructive pulmonary disease with and without lung cancer. *Cancer Prev Res (Phila)*. 2012;5:365-373.
- Wilk JB, Walter RE, Laramie JM, Gottlieb DJ, O'Connor GT. Framingham heart study genome-wide association: results for pulmonary function measures. *BMC Med Genet*. 2007;8:58.
- Haruju TH, Peltoniemi MJ, Ryttilä PH, et al. Glutathione S-transferase omega in the lung and sputum supernatants of COPD patients. *Respir Res*. 2007;8:48.
- Wang L, Xu J, Ji C, et al. Cloning, expression and characterization of human glutathione S-transferase Omega 2. *Int J Mol Med*. 2005;16:19-27.
- Board PG, Coggan M, Chelvanayagam G, et al. Identification, characterization, and crystal structure of the omega class glutathione transferases. *J Biol Chem*. 2000;275:24798-24806.
- Xiao W, Loscalzo J. Metabolic responses to reductive stress. *Antioxid Redox Signal*. 2020;303:359-363.
- Terayama M, Yamada K, Hagiwara T, et al. Glutathione S-transferase omega 2 regulates cell growth and the expression of E-cadherin via post-transcriptional down-regulation of  $\beta$ -catenin in human esophageal squamous cells. *Carcinogenesis*. 2020;41:875-886.
- Reis-Fiho JS, Simpson PT, Martins A, Preto A, Gärtner F, Schmitt FC. Distribution of p63, cytokeratins 5/6 and cytokeratin 14 in 51 normal and 400 neoplastic human tissue samples using TARP-4 multi-tumor tissue microarray. *Virchows Arch*. 2003;443:122-132.
- Arsalane K, Broekaert F, Knoop B, Wiedig M, Toubeau G, Bernard A. Clara cell specific protein (CC16) expression after acute lung inflammation induced by intratracheal lipopolysaccharide administration. *Am J Respir Crit Care Med*. 2000;443:122-132.
- Mason RJ, Greene K, Voelker DR. Surfactant protein A and surfactant protein D in health and disease. *Am J Physiol*. 1998;275:L1-L13.
- Sung YE, Cho U, Lee KY. Peripheral type squamous cell carcinoma of the lung: clinicopathologic characteristics in comparison to the central type. *J Pathol Transl Med*. 2020;54:290-299.
- Kato M. Multi-layered prevention and treatment of chronic inflammation, organ fibrosis and cancer associated with canonical WNT/ $\beta$ -catenin signaling activation (Review). *Int J Mol Med*. 2018;42:713-725.
- Carlier FM, Dupasquier S, Ambroise J, et al. Canonical WNT pathway is activated in the airway epithelium in chronic obstructive pulmonary disease. *EBioMedicine*. 2020;61:103034.
- Lehwald N, Tao GZ, Jang KY, et al.  $\beta$ -Catenin regulates hepatic mitochondrial function and energy balance in mice. *Gastroenterology*. 2012;143:754-764.
- Otsubo T, Yamada K, Hagiwara T, et al. DNA hypermethylation and silencing of PITX1 correlated with advanced stage and poor postoperative prognosis of esophageal squamous cell carcinoma. *Oncotarget*. 2017;8:84434-84448.
- Hu YC, Sidransky D, Ahrendt SA. Molecular detection approaches for smoking associated tumors. *Oncogene*. 2002;21:7289-7297.
- Mukherjee B, Salavaggione OE, Pellemounter LL, et al. Glutathione S-transferase omega 1 and omega 2 pharmacogenomics. *Drug Metab Dispos*. 2006;34:1237-1246.
- Haddad JJ. A redox microenvironment is essential for MAPK-dependent secretion of pro-inflammatory cytokines: modulation by glutathione (GSH/GSSG) biosynthesis and equilibrium in the alveolar epithelium. *Cell Immunol*. 2011;270:53-61.
- Lie Z, Shen S, Zhao X, et al. Activating  $\beta$ -catenin/Pax6 axis negatively regulates osteoclastogenesis by selectively inhibiting phosphorylation of p38/MAPK. *FASEB J*. 2019;33:4236-4247.
- Zhu J, Schwörer S, Berisa M, et al. Mitochondrial NADP(H) generation is essential for proline biosynthesis. *Science*. 2021;372:968-972.
- Li XQ, Yang XL, Zhang G, et al. Nuclear  $\beta$ -catenin accumulation is associated with increased expression of Nanog protein and predicts poor prognosis of non-small cell lung cancer. *J Transl Med*. 2013;11:114.
- Rapp J, Jaromi L, Kvell K, et al. WNT signaling - lung cancer is no exception. *Respir Res*. 2017;18:167.
- Rosa VD, Iommelli F, Monti M, et al. Reversal of warburg effect and reactivation of oxidative phosphorylation by differential inhibition of EGFR signaling pathways in non-small cell lung cancer. *Clin Cancer Res*. 2015;21:5110-5120.

**How to cite this article:** Sumiya R, Terayama M, Hagiwara T, et al. Loss of GSTO2 contributes to cell growth and mitochondria function via the p38 signaling in lung squamous cell carcinoma. *Cancer Sci*. 2021;00:1-10. doi:[10.1111/cas.15189](https://doi.org/10.1111/cas.15189)